(22) and the bipolaron-mediated two-component superconductivity (23, 24). In particular, deformation-induced charge transfer could provide the mechanism for a polaron mostly dressed by electron and thus having a small mass (25). More extensive studies of this nonlinear electron-lattice coupling could lead to a better understanding of the effect of electron correlation on various properties of oxides including ferroelectricity and superconductivity.

REFERENCES AND NOTES

1. P. W. Anderson, *Science* **235**, 1196 (1987).
2. F. C. Zhang and T. M. Rice, *Phys. Rev. B* **37**, 3759 (1988).
3. A. R. Bishop, R. L. Martin, K. A. Müller, Z. Tesanovic, *Z. Phys. Sect. B* **76**, 17 (1989).
4. S. K. Kurtz, J. R. Hardy, J. W. Flocken, *Ferroelectrics* **87**, 29 (1988).
5. A. R. von Hippel, *J. Phys. Soc. Jpn.* **28** (suppl.), 1 (1970).
6. R. E. Cohen and H. Krakauer, *Phys. Rev. B* **42**, 6416 (1990).
7. L. T. Hudson, R. L. Kurtz, S. W. Robey, D. Temple, R. L. Stockbauer, *ibid.* **47**, 1174 (1993).
8. A. Fujimori, personal communication.
9. T. Neumann, G. Borstel, C. Scharfschwerdt, M. Neumann, *Phys. Rev. B* **46**, 10623 (1992).
10. J. B. Torrance, J. E. Vazquez, J. J. Mayerle, V. Y. Lee, *Phys. Rev. Lett.* **46**, 253 (1981).
11. J. Hubbard and J. B. Torrance, *ibid.* **47**, 1750 (1981).
12. E. Dagotto and A. Moreo, *Phys. Rev. D* **31**, 865 (1985).
13. W. P. Su, J. R. Schrieffer, A. J. Heeger, *Phys. Rev. B* **22**, 2099 (1980).
14. S. Mazumdar and S. N. Dixit, *Phys. Rev. Lett.* **51**, 292 (1983).
15. J. E. Hirsch, *ibid.*, p. 296.
16. A. Bussmann-Holder, H. Buttner, A. Simon, *Phys. Rev. B* **39**, 207 (1989).
17. S. Ishihara, T. Egami, M. Tachiki, in preparation.
18. H. Bilz, G. Benedek, A. Bussmann-Holder, *Phys. Rev. B* **35**, 4840 (1987).
19. A. Bussmann-Holder, H. Bilz, G. Benedek, *ibid.* **39**, 9214 (1989).
20. K. Yonemitsu, A. R. Bishop, J. Lorenzana, *Phys. Rev. Lett.* **69**, 965 (1992).
21. J. Mustre-de Leon *et al.*, *ibid.* **68**, 3236 (1992).
22. A. Bussmann-Holder, in preparation.
23. R. Micnas, J. Ranninger, S. Robaszkiewicz, *Rev. Mod. Phys.* **62**, 113 (1990).
24. Y. Bar-Yam, *Phys. Rev. B* **43**, 359 (1991); *ibid.*, p. 2601.
25. J. E. Hirsch, *ibid.* **47**, 5351 (1993).

26. We are grateful to R. E. Cohen, A. Bussmann-Holder, A. Fujimori, Y. Ohta, S. Maekawa, E. Mele, H. Matsumoto, T. Koyama, and S. Takahashi for useful discussions. Supported by the Ministry of Education, Science, and Culture, Japan (Grant-in-Aid), the Office of Naval Research (N00014-91-J-1036), and the National Science Foundation (DMR90-01704 and DMR91-20668).

20 May 1993; accepted 28 July 1993

Molecular Dynamics of Adsorption and Segregation from an Alkane Mixture

T. K. Xia and Uzi Landman

Adsorption and segregation of *n*-hexadecane molecules from an equal by weight mixture of *n*-hexadecane and *n*-hexane to an Au(001) surface at 315 kelvin are studied with the use of molecular dynamics simulations. Preferential adsorption of *n*-hexadecane at the solid-to-liquid interface together with subsequent layer-by-layer growth of an ordered, wetting interface were observed. The long chains penetrate and adsorb at the interfacial layer by means of a sequential segmental mechanism involving end-segment anchoring and displacive desorption of preadsorbed *n*-hexane molecules.

The dynamic, thermodynamic, structural, and compositional properties of liquids and liquid mixtures can be significantly modified by surfaces and by confinement to narrow pores or films (*1–6*). In particular, surface segregation, or preferential adsorption, of long-chain molecules from a homologous polymer mixture of long- and short-chain components is a commonly observed phenomenon that is of considerable interest (*2–6*). Applications include adhesion, lubrication, colloidal stability and flocculation, chromatographic separation, the properties of plasticized polymeric materials (for which the concentration of the plasticized or reinforcing filler at the surface may be different from that in the interior), and the biocompatibility of artificial internal organs.

Whereas the kinetics and chain-length dependence of adsorption and wetting from polymer mixtures have been investigated extensively (*3–9*), issues pertaining to the dynamics of such processes are rather complex and have only recently been addressed experimentally and theoretically (*3*). Computer-based modeling and simulations open new avenues for investigation of the structure, energetics, and dynamics of complex liquids, as well as other materials systems (*10–13*). We report results of large-scale molecular dynamics (MD) simulations of surface segregation from an initially homogeneous alkane mixture (*14, 15*)—*n*-hexadecane (*n*-$C_{16}H_{34}$) and *n*-hexane (*n*-C_6H_{14})—which exhibits preferential adsorption of the long-chain molecules, occurring by means of a layer-by-layer epitaxial wetting. Furthermore, the simulations reveal that the atomic-scale dynamical adsorption mechanism involves sequential, segmental, reptation-like penetration and adsorption processes. Such a mechanism has been proposed and discussed recently in the context of experimental studies of adsorption-desorption kinetics of polymer chains at a solid surface (*3, 4, 7*).

In the MD simulations, which consist of the integration of the Newtonian equations of motion, we have investigated a 1:1 (by weight) mixture of *n*-hexane (400 molecules) and *n*-hexadecane (150 molecules), modeled with use of alkane interaction potentials, including dihedral, bond-angle, and nonbonded interactions. These potentials have been tested and used successfully in previous studies of bulk and interfacial liquid alkane systems (*11, 16–18*). The interactions between the CH_2 and CH_3 segments of the alkane molecules and a static crystalline Au(001) surface were modeled (*11, 17*) with 6-12 Lennard-Jones (LJ) potentials, where the parameters were fitted to experimentally estimated desorption data (the same segmental adsorption energy was assumed for both molecules). The strength of the interaction between a molecular segment and a gold atom is three times larger than that of the nonbonded intersegment interaction (*11, 17, 19*). The calculational cell, whose dimensions in the x and y directions, parallel to the solid surface, were 61.2 Å, was replicated in these directions with periodic boundary conditions; however, no periodicity was applied along the normal (z) direction.

In the first stage of the simulation, the mixture was prepared by means of a procedure described previously (*11*) that involved prolonged ($>10^3$ ps) equilibration of a homogeneous free mixture at a high temperature (450 K) followed by the cooling and adsorption of the mixture to form a liquid film at 315 K, which is above the melting temperature of either of the two components (291 and 178 K for the C_{16} and C_6 alkanes, respectively) but below their boiling points. The simulations were performed in the canonical (isothermal) ensemble, with infrequent thermalization by means of the scaling of particle velocities. The equations of motion were integrated with a 5th order predictor-corrector algorithm (*13*), with a time step $\Delta t = 3.86 \times 10^{-15}$ s, and the preferential adsorption process was simulated for 8 ns.

The total segmental density profile (ρ_s) (Fig. 1A, solid line) was calculated at the end of the simulation and exhibits density oscillations corresponding to interfacial layering of the film next to the solid-liquid interface, together with a tailing of the density at the liquid-vapor interface (*11*). The segmental density-difference profile

School of Physics, Georgia Institute of Technology, Atlanta, GA 30332.

$[\delta\rho_s = \rho_s(C_{16}H_{34}) - \rho_s(C_6H_{14})]$ (Fig. 1A, dashed line) and the ρ_s profiles of the individual components of the mixture (Fig. 1B) show preferential adsorption of the long-chain molecules at the solid-liquid interface and depletion of their concentration at the liquid-vapor interface (compare $\delta\rho_s$ at the end of the simulation to that at the start, the latter shown in the inset to Fig. 1A; see also Fig. 2).

At the solid-liquid interfacial layered region, the molecules, particularly the longer chains, lie preferentially parallel to the surface (Fig. 1C). In the segregated state (Figs. 1C and 2B), the first (and second, not shown) adsorbed layer possessed a high degree of intermolecular order with the $C_{16}H_{34}$ molecules oriented parallel to each other in patches (lamellae), but no such intermolecular ordering was seen in the initial, mixed state (Fig. 2A). The structural characteristics of the interfacial adsorbed alkane film revealed by our simulations are in agreement with the conclusions of early calorimetric studies (*20, 21*) (in which the preferential alignment of *n*-alkane molecules parallel to the solid surface was deduced), with more recent observations of lamellae structures in adsorbed alkane films done with scanning tunneling microscopy (*22*), and with previous simulations (*23*).

These structural features are governed by energetic and entropic contributions to the free energy of the system. A simple geometric packing consideration, with the length parameters of the alkane LJ potentials used in our simulations, shows that for hexadecane, the density of segments in a layer with all molecules confined to the layer and lying parallel to each other is over twice that obtained for a configuration in which only the end segment of each molecule is in the layer (that is, molecules oriented at an angle to the surface plane). Consequently, the preferential parallel alignment of molecules in the interfacial layer results in a stronger bonding interaction with the solid substrate, compensating for the loss in configurational entropy. The lamellae structure (Fig. 2B), exhibiting patches of intermolecular order oriented at an angle with respect to each other, may be a result of entropic contributions and may be associated with the segregation process itself and barriers for reorientation of the patches with respect to each other (which would involve a highly cooperative process).

In the segregated state, the diffusion of the hexadecane molecules at the solid-liquid interfacial region was practically quenched, increasing monotonically toward the liquid-vapor interface (Fig. 1D). Overall, the diffusion of the shorter chains was larger than that of the longer ones, exhibiting a significant enhancement of the

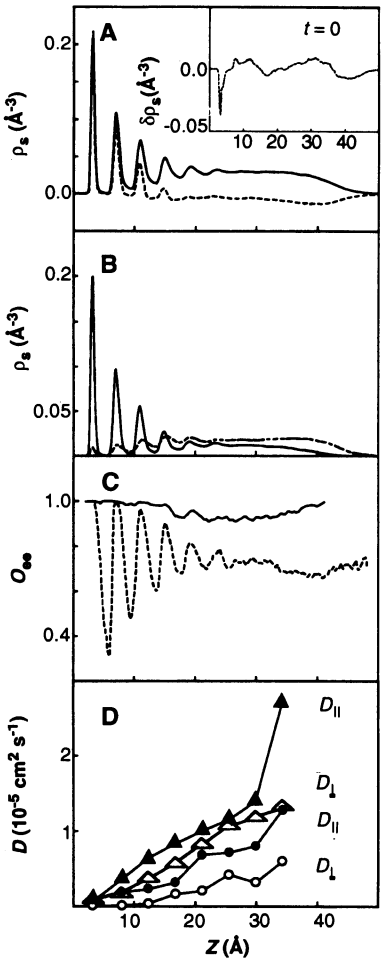

Fig. 1. Properties of the film of adsorbed alkanes at the end of an 8-ns simulation (averaged over the last 150 ps). (**A**) Total segmental density profile (solid line) and $\delta\rho_s = \rho_s(C_{16}H_{34}) - \rho_s(C_6H_{14})$ (dashed line). (**Inset**) $\delta\rho_s$ at $t = 0$. (**B**) Partial ρ_s profiles for *n*-$C_{16}H_{34}$ (solid) and *n*-C_6H_{14} (dashed). (**C**) Order parameter $O_{ee} = 1 - \langle(\mathbf{R}_{ee}\cdot\hat{\mathbf{z}})^2\rangle/R_{ee}^2$, where $\mathbf{R}_{ee}$ is the molecular end-to-end vector and $\hat{\mathbf{z}}$ is the unit normal to the surface. Angular brackets denote averaging over molecules whose center of mass is located in the interval $z \pm \Delta z$. Solid and dashed line correspond to *n*-$C_{16}H_{34}$ and *n*-C_6H_{14}, respectively. (**D**) Parallel, ($D_{||}$) (filled) and normal ($D_\perp$) (open) diffusion coefficients for *n*-hexadecane (circles) and *n*-hexane (triangles).

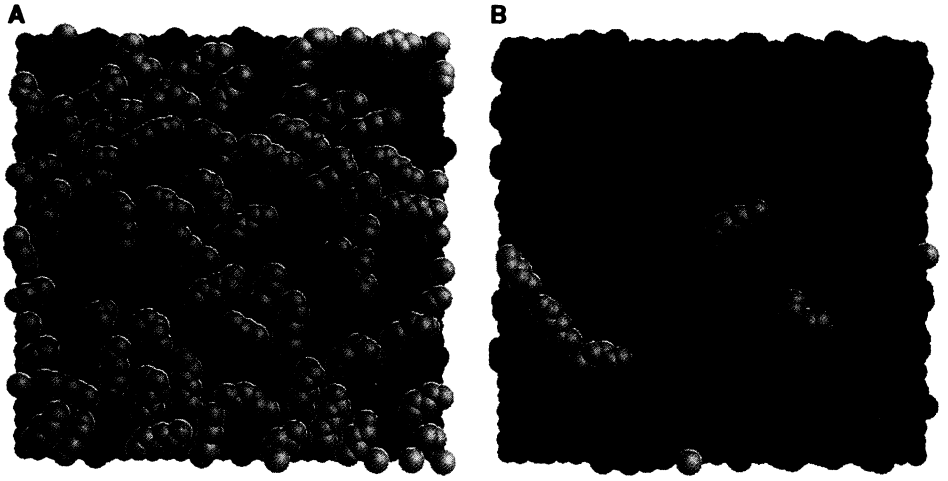

Fig. 2. Configurations of molecules in the first layer at (**A**) $t = 0$ and (**B**) $t = 8$ ns. The *n*-C_6H_{14} and *n*-$C_{16}H_{34}$ molecules are depicted in green and blue, respectively.

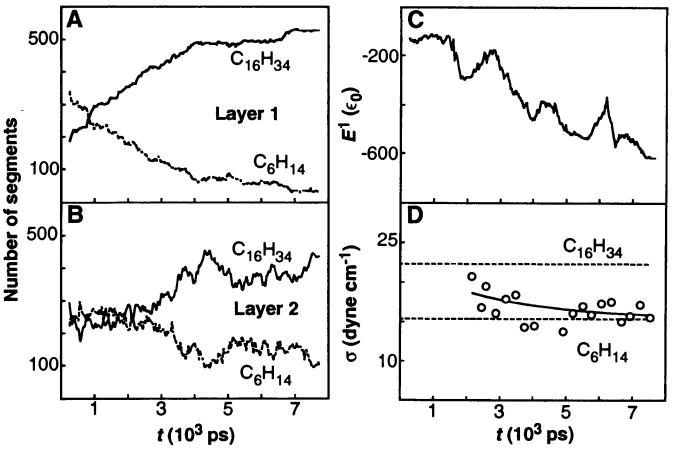

Fig. 3. Time evolution of the adsorbed mixture. (**A**) Number of segments belonging to *n*-$C_{16}H_{34}$ (solid) and *n*-C_6H_{14} (dashed) molecules in layer 1 of the solid-liquid interface. (**B**) Same as (A) for layer 2. (**C**) Total energy of segments in the first interfacial layer in units of ϵ_0, where $\epsilon_0 = 72$ K. (**D**) Surface tension σ at the liquid-vapor interface of the film mixture. Dashed lines denote the surface tensions determined for the pure components. The solid line represents fit described in (*25*).

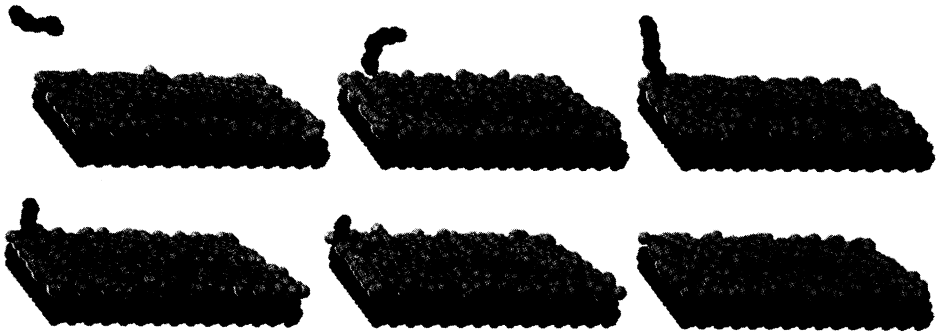

Fig. 4. Selected snap-shots of the adsorption of an n-$C_{16}H_{34}$ molecule (blue) from its starting position in the mixture (top left corner). The sequence illustrates end-segment anchoring to the Au(001) surface (red) and sequential segmental adsorption of the molecule accompanied by displacive desorption of short-chain molecules in the preadsorbed first layer (long and short chains in the first layer are depicted in green). For clarity, other molecules of the system are not shown. The sequence starts at the top left and ends at the bottom right. The time interval between the successive configurations is 30 ps.

parallel diffusion constant near the liquid-vapor interface (*11*).

The surface segregation process of the longer chain molecules exhibited a layer-by-layer "epitaxial" mechanism (Fig. 3, A and B). First, n-hexadecane wets the solid surface (layer 1 for $t \lesssim 4$ ns) at an average rate of 1.2×10^6 molecules s^{-1} Å^{-2}, at which point the completion of the wetting of the layer slows significantly [initially, the ratio of the number of molecules in the first layer was $n_1(C_{16}H_{34})/n_1(C_6H_{14}) = 13/56$, corresponding to an almost equal number of segments for the two components, whereas at $t = 8$ ns, the ratio was 33/5]. The segregation rate into the second solid-liquid interfacial layer is smaller, enhanced by the progressing preferential segregation and intermolecular ordering in the underlying first layer. The energetics of the process exhibits an overall lowering of the total energy in the first interfacial layer (E^1) (Fig. 3C). The oscillatory character of E^1 is associated with stages of penetration into the layer and intermolecular ordering in the layer during the segregation process together with segregation processes in the second adsorbed layer. The variation in the liquid-vapor surface tension of the film, approaching that of C_6H_{14} in the final state, is associated with the enrichment of the interface by short-chain molecules. The preferential adsorption of the longer chain molecules to the solid surface is driven by a lowering of the energy associated with better packing and intermolecular ordering at the solid-liquid interface (Fig. 2B), which compensates for the loss of conformational and mixing entropy upon selective adsorption, as well as by the lowering of the surface tension at the liquid-vapor interface accompanying the increase in the fraction of shorter chain molecules in this region.

The particle trajectories (Fig. 4) suggest that adsorption of the n-$C_{16}H_{34}$ molecules is initiated by their anchoring to the solid by end-segment penetration, followed by sequential, segmental, reptation-like adsorption of the molecule, inducing displacive desorption of preadsorbed short-chain molecules. Analysis of the time histories of the simulation shows that the anchoring process usually occurred at a preexisting "vacancy" in the layer, generated by intralayer fluctuations as well as by short-chain partial desorption events. The above dynamical mechanism correlates with the decrease in adsorption rate as the process of segregation to the surface evolves (Fig. 3A): As the solid-liquid interfacial layer becomes enriched by the well-ordered long-chain molecules, the availability of anchoring sites is reduced. Furthermore, adsorption of an incoming molecule requires structural rearrangements at the interface, with the corresponding free-energy barriers increasing as the coverage and ordering at the surface progress.

Understanding of chain dynamics and of the atomic-scale mechanisms that govern interfacial processes is at a very early stage: For example, current theories of random sequential adsorption (*24*) are limited to consideration of the adsorption of particles having a fixed, compact shape rather than the adsorption of chains. We expect that the results of our MD simulations will provide an impetus for further critical, controlled experiments and improved fundamental understanding of these phenomena, including investigation of a range of chain lengths and concentrations as well as studies of issues related to the history of the system [that is, equilibrium versus trapped nonequilibrium states (*3*)].

REFERENCES AND NOTES

1. J. N. Israelachvili, *Intermolecular and Surface Forces* (Academic Press, London, 1985).
2. S. Granick, *Science* **253**, 1374 (1991).
3. _____, in *Physics of Polymer Surfaces and Interfaces*, I. C. Sanchez, Ed. (Butterworth-Heinemann, Boston, MA, 1992), p. 227.
4. P. G. de Gennes, *Adv. Colloid Interface Sci.* **27**, 189 (1987).
5. M. A. Cohen Stuart, T. Cosgrove, B. Vincent, *ibid.* **24**, 143 (1986).
6. A. Takahashi and M. Kawaguchi, *Adv. Polym. Sci.* **46**, 1 (1982).
7. P. Frantz and S. Granick, *Phys. Rev. Lett.* **66**, 899 (1991).
8. H. E. Johnson and S. Granick, *Science* **255**, 966 (1992).
9. U. Steiner, J. Klein, E. Eiser, A. Budkowski, L. J. Fetters, *ibid.* **258**, 1126 (1992).
10. K. Kremer and G. S. Grest, *Computer Simulation of Polymers*, R. J. Roe, Ed. (Prentice-Hall, Englewood Cliffs, NJ, 1991), p. 167.
11. T. K. Xia, J. Ouyang, M. W. Ribarsky, U. Landman, *Phys. Rev. Lett.* **69**, 1967 (1992).
12. U. Landman, R. N. Barnett, W. D. Luedtke, *Philos. Trans. R. Soc. London Ser. A* **341**, 337 (1992), and other articles in that issue; F. F. Abraham, *Adv. Phys.* **35**, 1 (1986).
13. M. P. Allen and D. J. Tildesley, *Computer Simulations of Liquids* (Clarendon, Oxford, U.K. 1987).
14. J. H. Hildebrand and J. W. Sweny, *J. Phys. Chem.* **43**, 297 (1939); J. H. Hildebrand, *ibid.*, p. 109.
15. M. L. McGlashan and K. W. Morcom, *Trans. Faraday Soc.* **57**, 581 (1961).
16. J. P. Ryckaert and A. Bellemans, *Discuss. Faraday Soc.* **66**, 95 (1978).
17. M. W. Ribarsky and U. Landman, *J. Chem. Phys.* **97**, 1937 (1992).
18. S. Leggetter and D. J. Tildesley, *Mol. Phys.* **68**, 519 (1989).
19. The value of the well depth $\epsilon = 0.429$ kcal mol^{-1} and the length parameter $\sigma = (\sigma_{Au} + \sigma_{CH_2})/2 = 3.28$ Å (determined by the Lorentz-Berthelot mixing rule) in the 6-12 LJ interaction potential between an alkane segment and a gold atom were chosen to yield an adsorption energy of ~1 kcal mol^{-1} per pseudoatom (CH_2 segment), in agreement with results obtained in thermal desorption studies (*11*, *17*). In an earlier study (*17*), the sensitivity of structural and dynamical properties of liquid hexadecane films interacting with metal surfaces was investigated as a function of the strength of the alkane-to-metal surface interaction potential. The results of that study indicate that the structural properties of the interfacial layer of the film pertinent to our current investigations are quite insensitive to certain variation (say a factor of 2) in the molecule-to-surface interaction strength.
20. A. J. Groszek, *Proc. R. Soc. London Ser. A* **314**, 473 (1970).
21. G. H. Findenegg and M. Liphard, *Carbon* **25**, 119 (1987).
22. J. P. Rabe and S. Buchholz, *Science* **253**, 424 (1991).
23. U. Landman, W. D. Luedtke, J. Ouyang, T. K. Xia, *Jpn. J. Appl. Phys.* **32**, 1444 (1993).
24. R. Dickman, J.-S. Wang, I. Jensen, *J. Chem. Phys.* **94**, 8252 (1991).
25. The solid line represents a fit according to
$$\sigma(t) = \sigma_\infty + (\sigma_0 - \sigma_\infty)e^{-(t - t_0)/\tau}$$
where $\sigma_\infty = 15.37$ dyne cm^{-1} is the surface tension for pure n-C_6H_{14}, $\sigma_0 = 18.83$ dyne cm^{-1} is the average of the surface tensions for pure n-C_6H_{14} and n-$C_{16}H_{34}$, $t_0 = 2.0 \times 10^3$ ps is the time at the start of the calculation of the surface tension, and $\tau = 2.85 \times 10^3$ ps is the relaxation time, estimated from the time-evolution curve of the number of n-C_6H_{14} molecules in the first adsorbed layer shown in (A) [assuming $n(t) = n_0e^{-t/\tau}$, where n_0 and $n(t)$ are the number of segments of n-hexane molecules in the first solid-liquid adsorbed layer at $t = 0$ and $t \geq 0$, respectively].

26. We acknowledge the assistance of C. L. Cleveland in preparing Figs. 2 and 4 and discussions with W. D. Luedtke. This research is supported by the U.S. Department of Energy, the National Science Foundation, and the Air Force Office of Scientific Research. Calculations were performed with CRAY-YMP and C-90 computers at the Pittsburgh Supercomputing Center.

19 April 1993; accepted 2 July 1993